Aust. J. Phys., 1995, **48**, 527–41

Measurement of Electrical Discharge Parameters Using Optical Fibres*

V. Everett, K. T. Jones, G. B. Scelsi and G. A. Woolsey

Optical Fibre Sensors Group, Department of Physics,
University of New England, Armidale, NSW 2351, Australia.

Abstract

A consequence of the development of optical fibre technology for communications has been the application of optical fibres to the sensing of a wide range of physical and chemical parameters. Many of the properties of fibres that are important for communications are significant for sensing: these include their insulating nature, their small dimensions, and their immunity to high voltage and electromagnetic radiation. These attributes are particularly significant for sensing electrical discharges, and this review presents a discussion of the potential of optical fibre sensing for discharge parameters, the results of some recent optical fibre measurements made on corona and glow discharges, and suggestions for other discharge probing approaches using optical fibres.

1. Introduction

A wide range of diagnostic techniques has been developed for discharge and plasma study (Huddlestone and Leonard 1965). These include electric and magnetic probes, optical and mass spectrometry, laser scattering, optical and microwave interferometry, schlieren analysis and laser Doppler anemometry. Most of these measuring techniques have limitations with either their range of application, their spatial resolution or their disturbance of the discharge environment, and experimentalists in the field of electrical discharges are always receptive to suggestions for new diagnostic approaches.

Optical fibre sensors have several attributes that make them attractive for discharge probing. As insulators, optical fibres create none of the electrical disturbance or breakdown problems often associated with metal probes, and their small dimensions mean that distortion of discharge structure is minimised. With many discharges occurring in environments which are electromagnetically noisy and which involve high voltages, signal transfer and processing through optical fibres provides significant benefits.

Optical fibre sensors essentially come in two forms; intrinsic and extrinsic. In the former, the fibre itself is the sensing element, and in the latter, fibres are used to transmit light to and from a separate sensing element. The sensors discussed here are intrinsic, with the quantity being measured modulating the light passing through the fibre to vary the phase, intensity or spectral distribution of the light.

* Refereed paper based on a contribution to the Third Japan–Australia Workshop on Gaseous Electronics and Its Applications, held in Yeppoon, Queensland, in July 1994.

0004-9506/95/030527$05.00

Prior to the development of our programme of research at the University of New England, application of optical fibres to gas discharge studies was confined to current measurement and light transfer in optical spectroscopy. Toroidal plasma currents have been measured by Faraday rotation in a single-mode fibre (Chandler and Jahoda 1985; Lassing *et al.* 1987), and optical fibre probes have been used to examine the light emitted from plasma sources such as those used for etching and magnetohydrodynamic (MHD) combustion (Jin *et al.* 1988; Simons 1984).

This paper reviews a range of approaches to the optical fibre sensing of electrical discharges, some of which have been successfully demonstrated in our laboratory, and some of which are presently under investigation. Discharge parameters and processes being examined include electric field, the corona wind, neutral gas temperature, charge density and chemical dissociation. The primary technique used in our work is that of optical fibre interferometry, and the following section provides a summary of the principles of optical fibre sensors based on that technique. Descriptions of our experimental approaches to the optical fibre sensing of discharges, and the results from measurements of some discharge parameters are then presented.

2. Interferometric Sensing

Single-mode optical fibres carry monochromatic light without altering its coherence characteristics and can therefore be used to assemble optical interferometers. In contrast to bulk-optics arrangements, fibre interferometers are free from the constraint of having light travelling along straight paths. Interferometer arms can go around bends, can be wound in coils and can extend over considerable lengths without being subjected to strict alignment and stability requirements.

All of the common unbound-beam interferometric configurations have a corresponding optical fibre version. Michelson, Mach–Zehnder, Fabry–Perot and Fizeau interferometers can all be readily assembled using couplers, splices and other fibre components which have become commercially available due to their application in optical telecommunications.

Fig. 1 shows the schematic arrangements of three commonly used optical fibre interferometers. The similarity to unbound-beam interferometers is apparent given that the 2×2 directional coupler is the optical fibre equivalent of a conventional 50% beam splitter. The Michelson interferometer normally relies on the Fresnel reflection at the cleaved ends of the two fibre arms, generated by the refractive index discontinuity between silica and air. Alternatively, the two fibre ends can be coated with metallic or dielectric films to increase the overall intensity impinging on the photodetector. In the Fabry–Perot case, the resonant cavity consists of a section of single-mode fibre which has been carefully cleaved at the two ends to provide optically flat and smooth surfaces. The two surfaces can be subsequently coated with a highly-reflective film to achieve the desired finesse, or can be left uncoated. In the latter case, due to the low reflectivity of the end surfaces, the device essentially behaves as a two-beam interferometer and is more appropriately called a Fizeau interferometer.

Because of the possibility offered by optical fibre technology to build compact, rugged and relatively cheap interferometers, a large number of optical fibre sensors based on interferometric techniques has been developed. A detailed review of

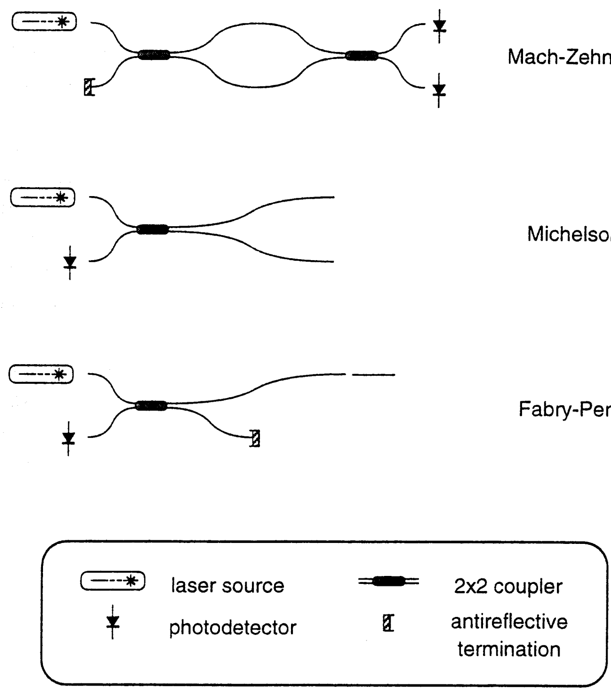

Fig. 1. Schematic diagrams of the three most commonly used optical fibre interferometers.

optical fibre interferometers and a discussion of their application to precision measurement has been presented by Jackson (1985).

The main drawback of optical fibre interferometric sensors is their intrinsic sensitivity to any physical parameter that affects the optical characteristics of the fibre, most significantly temperature. A change in temperature affects the optical path length of the fibre by altering both its physical length and the index of refraction of the fibre material. For a typical silica fibre the photo-thermal sensitivity is of the order of 100 $\mathrm{rad\,m^{-1}\,K^{-1}}$. If temperature is not the measurand of interest, care must be taken to minimise these unwanted effects.

Even if temperature is the object of the measurement, it is still a problem to confine temperature changes to the section of the fibre which traverses the region of interest, while shielding the rest of the fibre from any external influence. In this respect, the Fabry–Perot configuration offers a considerable advantage, as the interferometer sensitive section can be tailored to the size of the region to be monitored. Any change in temperature taking place within the optical fibre coupler or any of its four arms does not affect the interferometer output signal and therefore no particular shielding is needed. In addition, the Fabry–Perot resonator can be placed far from the detection system, since the leading fibre does not play any role in the performance of the device.

Temperature measurements which make use of optical fibre interferometers can be divided into two classes: point measurement and integrated measurement. Point measurements aim to obtain a direct evaluation of the temperature of a gas, a liquid or a solid object at a particular point in space, in analogy with what is achieved for instance with a thermocouple probe. Point probes based on the intrinsic dependency of the fibre optical pathlength on temperature would exhibit a very low sensitivity, this being directly proportional to the probe length. Other sensing schemes are therefore necessary.

An alternative approach is taken with integrated temperature measurement. Here the measuring arm of the optical fibre interferometer traverses the entire region of interest, which in general exhibits a non-uniform temperature distribution. The infinitesimal optical path length of each elemental section of the fibre is proportional to the local temperature achieved by the fibre. The interferometer response is therefore determined by the integral sum of all these infinitesimal contributions, evaluated across the measurement region. After completion of a number of such integrated measurements, each corresponding to a different position of the fibre within the region of interest, mathematical techniques similar to the ones used in axial tomography can be applied to recover the spatial temperature distribution. In the special case where the temperature distribution has circular cylindrical symmetry, the problem reduces to the evaluation of an inverse Abel transform (Scelsi *et al.* 1994).

3. Sensing of Corona Discharges

(3a) Corona Wind

An important characteristic of a corona discharge is the corona wind, produced by momentum transfer between ions moving rapidly away from the high voltage point and neutral gas molecules. The motion of the neutrals is enhanced by a pressure drop around the point electrode (Yabe *et al.* 1978). The corona wind takes the form of a relatively narrow jet. Since the gas flow of the corona wind is generated by ionisation around the point, the wind speed depends on current and electrode geometry. The speed of the corona wind has been found both theoretically and experimentally to be proportional to the square root of the current (Yabe *et al.* 1978; Sigmund 1982). For a wide range of geometries and discharge systems, the velocity of the wind is around a few metres per second and the wind has been detected up to 0·5 m away from the discharge gap (Woolsey *et al.* 1991).

The corona wind, sometimes called the ionic or electric wind, is creating interest among researchers, as more and more applications are found for both corona discharges and the corona wind. Coronas provide an abundant source of ions of the same polarity as the high voltage point or wire, and are used for particle charging in devices such as photocopiers and electrostatic precipitators. On the other hand, unwanted coronas occur at points and sharp edges in high voltage switchgear and power lines, and can lead to degradation of gas and solid insulation, corrosion of conductors and to sparking. The corona wind has excited interest in several practical areas: as a compact source of air flow for heat transfer applications (Bradley and Hoburg 1985; Asakawa 1976; Kibler and Carter 1974); to assist in the uniform distribution of heat in ovens for commercial bread baking (Kulacki and Daumenmier 1978; Curry 1987); and as a contributing factor in electrostatic precipitation. It may also have a role to play in the deposition of solid SF_6 dissociation products in high voltage devices which use SF_6 for insulation.

(3b) Measurement of the Corona Wind

To measure the velocity of the corona wind, Pitot tubes (Sato 1980), rotating cup anemometers (Large and Pierce 1957) and hot wire anemometers (Thanh 1979) have been used. These methods restrict measurements to the area outside the electrode gap as they require the introduction of bulky or conductive instruments into the gap: these disturb the electric field and hence the wind velocity.

One optical method which has been employed to study the corona wind within the gap is laser Doppler anemometry (LDA) (Sato 1980; Teisseyre *et al.* 1982). In LDA, two light beams of equal intensity are focused on a small probe volume in the discharge gap. Scattering particles of dimensions in the range 1–5 μm are introduced into the gap to scatter the light (Drain 1980). The light scattered from the moving particles in the probe volume is frequency shifted due to the Doppler effect and this scattered light is focused onto a photomultiplier. Since the flow direction of the particles relative to the beam direction is different for the two beams, a beat frequency is produced which is proportional to the particle velocity, and hence to the corona wind velocity. Corona wind velocity measurements obtained using LDA are in error, however, because scattering particles introduced into the corona gap become charged, so that they derive a velocity component due to drift in the electric field. As a result, LDA measurements overestimate the velocity of the corona wind, by up to 30% (Sato 1980; Woolsey *et al.* 1991).

(3c) Optical Fibre Anemometer

Optical fibre systems have small dimensions, are non-conductive and do not require the use of scattering particles. They therefore overcome the major problems associated with conventional wind-speed measuring devices for corona study. The basis of velocity measurement using our optical fibre sensor (Lamb and Woolsey 1994) is similar to that of a hot-wire anemometer, i.e. convective cooling. The system shown in Fig. 2 illustrates the use of a Michelson interferometer arrangement: we also have successfully used Mach–Zehnder and Fabry–Perot optical fibre interferometers for corona wind measurement. Light from a 4 mW He–Ne laser is launched into one arm of an ACROTEC 2×2, 633 nm single mode, bi-directional coupler, which provides equal intensities in the two output fibre arms of the coupler. The single-mode fibre of the sensing arm is placed across the corona gap, normal to the wind direction, while the second output fibre is the reference arm of the Michelson interferometer. The end of each of the sensing and reference fibres is cleaved, with the result that approximately 4% reflectance occurs at each end. A short length of the fibre in the sensing arm is heated by a 200 ms pulse from a 13 W CO_2 laser (SYNRAD): with the laser output placed 40 cm from the fibre, the spot width at the fibre is 4 mm. The maximum temperature reached by the fibre is controlled by the convective effect, and therefore the speed, of the corona wind. The signal from the photodiode is amplified and fed to a universal counter (Hewlett Packard 5316A) which is gated only during the laser pulse: this means that fringes are counted only during the heating period. As described in Section 2, the number of interference fringes counted is a function of the rise in temperature of the fibre and hence of the wind speed. The experimental arrangement of Fig. 2 allows the CO_2 laser/fibre system to probe any part of the discharge gap.

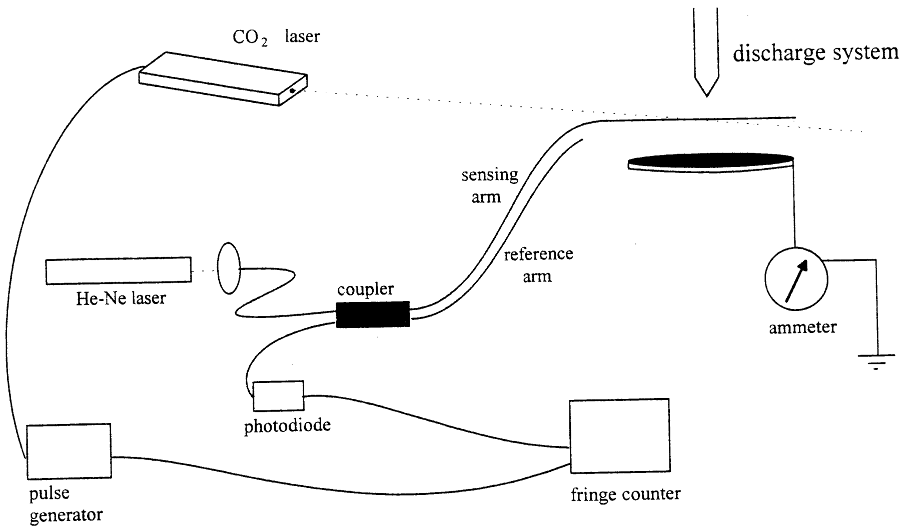

Fig. 2. Michelson interferometer and CO2 laser arrangement used for corona wind sensing.

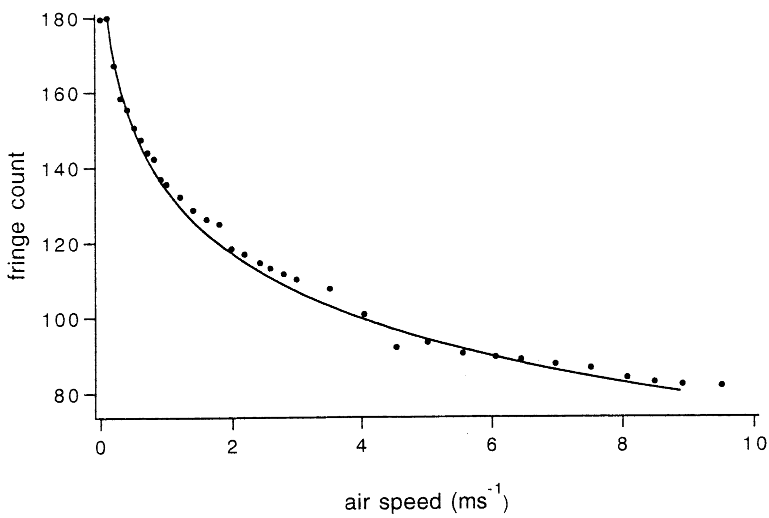

Fig. 3. Calibration curve showing fringe count versus air speed for the corona-wind sensor. The curve was obtained by fitting to the experimental data theoretical expressions relating the convection coefficient for the fibre to the fringe count and wind speed (Lamb and Woolsey 1994).

In order to convert fringe data into wind speed, the measuring system must be calibrated. This was done by placing the sensing fibre in the air flow from a 5 mm diameter nozzle, and recording fringe counts for a range of known flow speeds, using the same pulse heating arrangement as for the corona measurements. Data were obtained for flow speeds in the range $0\cdot1$ to $10\ \mathrm{m\,s^{-1}}$, corresponding to volume flows through the nozzle of 1 to 12 litres per minute. Volume flows and speeds were measured using a set of three rotameters (Gilmont Shielded Flowmeters) with a precision of $\pm2\%$. The calibration curve of Fig. 3 shows how an increase in convection with faster flow speed decreases the fibre temperature and hence the number of fringes recorded.

(3d) Results and Discussion

Corona wind speed patterns are shown in Fig. 4 for (*a*) point-plate and (*b*) point–grid electrode configurations. For each, the point electrode was a 6° hyperboloid, the inter-electrode spacing was 20 mm, the current was 20 μA, and the point was at a positive potential of 13·5 kV. The plate and grid were 40 mm in diameter. The plotted data were obtained by scanning radially in 0·5 mm steps for axial positions 0·5 mm apart. At each point of measurement, an average of the fringe counts was obtained for five separate fibre-heating pulses.

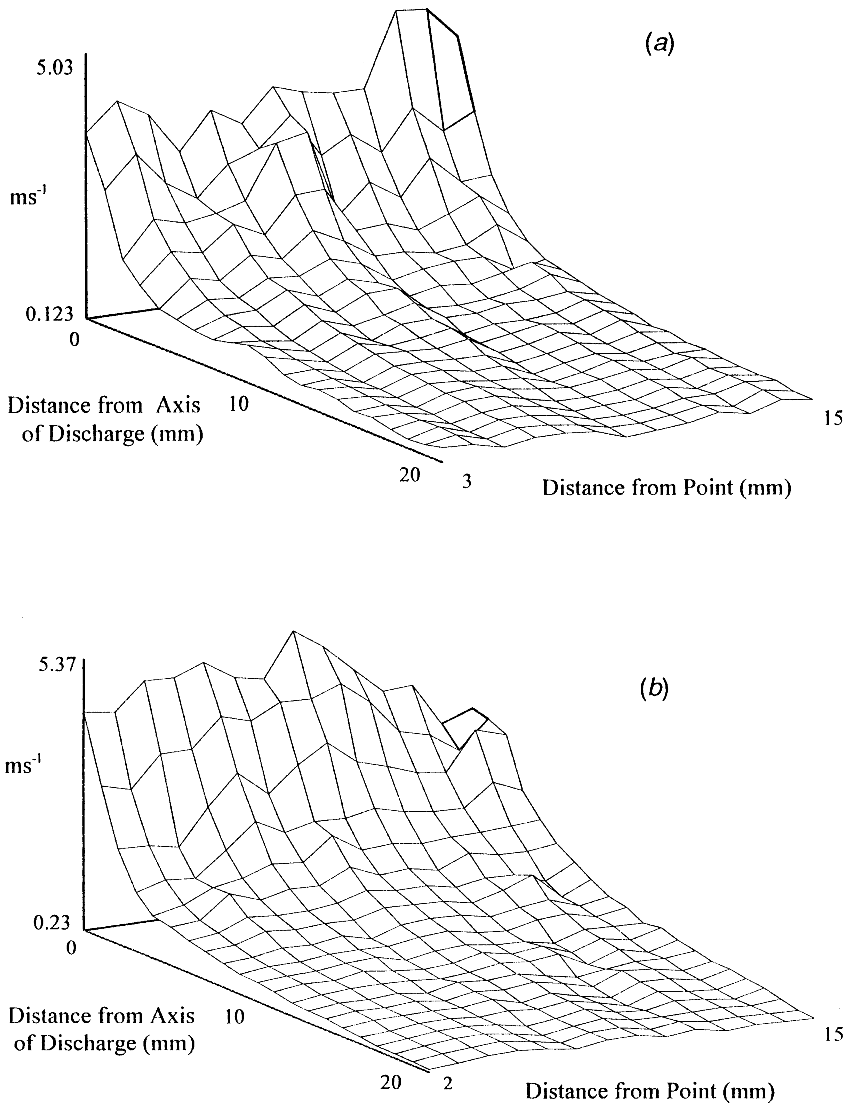

Fig. 4. Patterns of corona wind speed for (*a*) point–plate and (*b*) point–grid electrode configurations, in air at 680 Torr (900 mbar) pressure and 30% relative humidity.

The radial profiles of the wind speed are seen to be substantially peaked, falling from around 5 $\mathrm{m\,s^{-1}}$ on-axis to $0\cdot5$ $\mathrm{m\,s^{-1}}$ within a radius of 15 mm. This result is accounted for by the nature of the wind generating mechanism: ions are accelerated in the electric field adjacent to the point electrode, with maximum momentum transfer taking place along the axis where the field is highest.

The on-axis wind speed appears to fall on approaching the grid, whereas it rises on approaching the plate. The apparent rise in wind speed at the plate may be caused by additional cooling brought about by a local increase in pressure in the region where the air strikes the plate: this would be interpreted by the sensor as an increase in wind speed.

A shortcoming of the sensor with its present configuration is its lack of directionality. This is a particular problem for measurement near surfaces where deflection of the wind occurs, and we believe it can be overcome by using a double probe arrangement. Such a sensing arrangement will aid the study of wind direction for coronas which have to be maintained within discharge chambers. For example, we plan to investigate the corona wind in SF_6 to obtain information on the distribution of the solid by-products that are produced in SF_6 discharges following dissociation processes. Such information has particular relevance for the design and maintenance of SF_6 switchgear and insulating systems.

(3e) Electric Field

Using the the Mach–Zehnder arrangement of Fig. 1, with a short length (20 mm) of piezoelectric film (polyvinylidene fluoride) bonded to the measuring fibre, we have measured electric fields in the corona gap (Woolsey *et al.* 1991). However, the relatively large film size which is needed to provide an acceptable sensitivity of 10 $\mathrm{kV\,cm^{-1}}$ per fringe is unsatisfactory. Sparking results when the sensing fibre/film combination is placed closer than 2 mm to the point electrode, the 20 mm film length significantly limits the resolution of the sensor, and it is likely that its relatively large surface area produces appreciable distortion of the electric field. Nevertheless, this optical fibre sensor does show promise for measuring the electric field in a corona, a critical discharge parameter whose measurement has always presented great difficulty. It should be possible to improve the performance of this fibre sensor for corona measurement, by thinly coating the polyvinylidene fluoride onto the sensing fibre.

(3f) Electric Charge

A corona gap is filled with ions of the same charge as the point electrode, drifting towards the plane electrode. Information on the density of these ions is useful when examining the behaviour of coronas, and for applications based on the charging effect of the ions, as in photocopiers and electrostatic precipitators. A possible optical fibre method of ion density measurement is one which uses a fibre Fabry–Perot interferometer with one reflecting surface in the form of an insulating membrane as one type of pressure-measuring device (Wolthuis *et al.* 1991). Charge on the outer membrane surface induces charge on the second surface of the interferometer and the resultant electrostatic force alters the cavity length. The ion density can be determined from the surface charging rate following the establishment of the corona, as measured by the rate of interferometric phase change.

4. Sensing of Glow Discharges

(4a) E/N in the Glow

The elastic and inelastic collision processes occurring in the various regions of a glow discharge depend critically on electron energy, which is a function of E/N, the ratio of electric field E to gas number density N. Profiles of N can be determined using a measurement of pressure in the discharge chamber together with spatially-resolved temperature measurements. We have developed an optical fibre sensor to probe the temperature distribution of a glow discharge (Scelsi *et al.* 1994).

(4b) Principle of the Temperature Sensor

In this measurement the optical fibre sensor measures the integral of the temperature distribution along a straight-line path within the heated volume of gas. After collecting a set of such integral measurements, it is then possible to recover the entire temperature distribution by means of a deconvolution method. Advantage is taken of the fact that the most common geometry for the containing vessel of an electrical discharge has cylindrical symmetry, so that the discharge temperature is a function only of the longitudinal coordinate z and the radial coordinate r and is independent of the azimuthal coordinate θ. This symmetry reduces the deconvolution problem to the evaluation of the inverse Abel transform.

Fig. 5 shows the circular cross section of the discharge volume perpendicular to the z axis. On such a plane the temperature is a function only of the radial coordinate r. The temperature outside the cylindrical region is assumed to be at a constant value T_0. With the sensing arm of an optical fibre interferometer placed on the cross-sectional plane at a distance y from the axis, the index of refraction of the silica fibre becomes a function of the position coordinate x, and the total change in optical path is given by an integral evaluated along the length of fibre within the circular cross section. It is assumed that each point of the fibre reaches thermal equilibrium with the surrounding neutral gas so that the temperature distribution along the fibre precisely duplicates the temperature distribution of the neutral gas.

The contribution to optical path length from each elemental section of the fibre is proportional to the local change in temperature as well as to the incremental length $\mathrm{d}x$. This can be written as

$$\mathrm{d}\phi = \Gamma[T(r) - T_0]\mathrm{d}x = \Gamma[T(r) - T_0]\frac{r\,\mathrm{d}r}{(r^2 - y^2)^{\frac{1}{2}}}\,, \qquad (1)$$

where Γ is the photo-thermal sensitivity defined in Section 2. The total phase shift ϕ is therefore given by

$$\phi(y) = 2\Gamma \int_y^R \frac{[T(r) - T_0]r\,\mathrm{d}r}{(r^2 - y^2)^{\frac{1}{2}}}\,. \qquad (2)$$

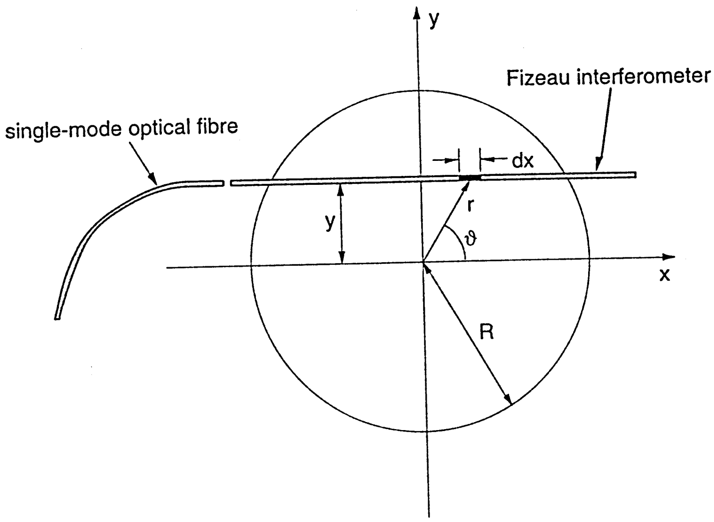

Fig. 5. Schematic diagram showing the location of the sensing arm of the optical fibre Fizeau interferometer used for the measurement of glow temperatures.

This is the Abel transform of the temperature distribution $T(r)$, which can therefore be expressed in terms of ϕ using the inverse transformation (Bracewell 1965)

$$[T(r) - T_0] = -\frac{1}{\pi\Gamma}\int_r^R \frac{\mathrm{d}\phi}{\mathrm{d}y}\frac{\mathrm{d}y}{(y^2 - r^2)^{\frac{1}{2}}}\,. \tag{3}$$

From measurements of phase shift ϕ for different fibre positions y, the integral in equation (3) can be evaluated for different values of r to provide the radial temperature profile $T(r)$. For a double-pass interferometer, such as a Michelson or Fizeau, the quantity Γ must be multiplied by 2, because a light beam passing through the sensing arm of the interferometer interacts twice with each element of the fibre.

(4c) Experimental Details

A Fizeau, or low-finesse Fabry–Perot, interferometer, as depicted in Fig. 1, was chosen for the glow temperature measurements, for the reasons discussed in Section 2. The optical spectrum of the He–Ne laser used in our experiment showed two or three longitudinal modes with a spacing of about 730 MHz. The multimode nature of the laser source required the optical path length of the interferometer to be made close to the laser cavity length, in order to maximise fringe visibility. Furthermore, the laser tube was thermally insulated from the room environment, to minimise mode drift during measurement. The phase shift detected by the photodiode was amplified and stored in a digital storage oscilloscope for further analysis.

The discharge and sensing fibre arrangement is sketched in Fig. 6. The glow discharge was established between two plane 42 mm diameter electrodes placed in a pair of 44 mm diameter coaxial cylindrical glass tubes, separated by a 2 mm gap. This gap allowed the introduction of the fibre interferometer, leaving the discharge undisturbed. The electrode separation and the sampling plane of the fibre between the electrodes could be altered by independently moving the electrodes. For each plane, the sensing fibre could be scanned across the discharge, thus allowing measurements to be made for different chords. The data presented here were obtained for a constant electrode separation of 150 mm, and the discharge was sampled at distances between 1 and 149 mm from the cathode. The whole arrangement shown in Fig. 6 was enclosed in a 75 mm diameter cylindrical vacuum chamber. The electrodes were connected to a high voltage supply through a 500 kΩ series resistor to prevent the glow proceeding to an arc discharge.

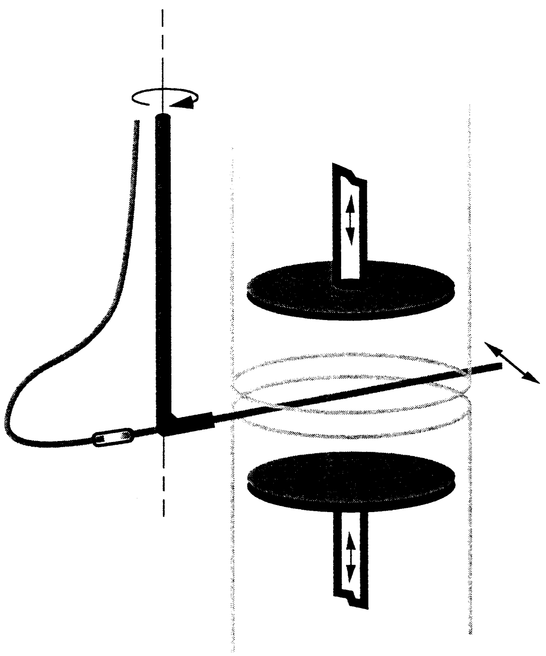

Fig. 6. Geometry of a fibre along a chord of the cross section of an axially symmetrical temperature distribution.

(4d) Results and Discussion

For several axial positions in an argon glow discharge at a pressure of 1 Torr (1·3 mbar) and a current of 4 mA, interferometer fringe shifts were measured for several chord positions to provide radial neutral gas temperature distributions. The temperature profiles near the electrodes were found to be relatively flat, because in these regions electrode conditions control the gas temperature. The cathode behaves as a relatively uniform heat source, and the anode as a cold heat sink. In the body of the discharge, the radial temperature distributions were found to decrease smoothly from the axis to the tube wall. In the positive column, they were essentially parabolic, in agreement with theory (Francis 1956). Fig. 7 shows the temperature distribution on the axis of the discharge, alongside the argon glow structure. In the body of the discharge, the gas neutrals gain their energy from the electrons, and the axial temperature profile closely reflects the mean energy of the electrons. At the cathode, which is heated by positive ion bombardment, the gas neutrals gain energy by conduction from the hot surface of the electrode. At the cold anode, the gas temperature falls, as the neutrals lose energy to the surface of that electrode.

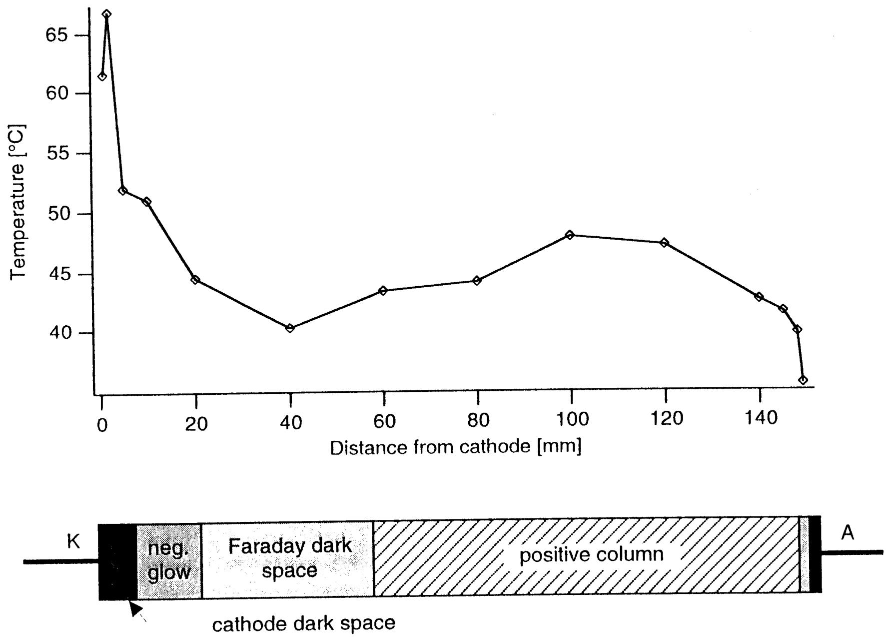

Fig. 7. Axial temperature profile measured in a glow discharge in argon at 1 Torr (1·3 mbar) pressure.

We examined the possibility that the rise in temperature measured near the cathode might be the result of positive ion bombardment of the fibre. The ion energies close to the cathode are up to 10^4 times the neutral particle energies, but their density is only around 10^{-6} of the neutral density. This suggests that the ion contribution to the fibre temperature should be small. The role of the ions in heating the sensing fibre was investigated experimentally by shielding the fibre from the cathode-directed ion beam. This was done by placing a narrow strip of dielectric material 1 mm from the fibre on the anode side. This caused no discernible disturbance to the discharge. Temperature measurements made with the shielded and unshielded optical fibre sensors yielded similar results within the limits of resolution of the sensing system, thus confirming that any ion contribution to the fibre heating was indeed small.

5. Chemical Sensing

Electrical discharges in gases can induce a complex range of chemical reactions. Molecular gases are dissociated and ionised, radicals are generated and a number of more or less stable gaseous and solid by-products is formed. Monitoring of these by-products is important for the study of the discharge dynamics as well as for practical applications of gas discharges. Many plasma-processing and plasma-etching systems use fluoride compounds, and an accurate control of the concentration of fluorine species generated by the glow discharge is essential for achieving high-quality and reproducible results. Spurious corona discharges occurring inside SF_6-filled switchgear and insulating systems cause a slow contamination of the original gas, with a consequent degradation of its dielectric properties. By monitoring the level of contamination, continuous information on dielectric efficiency is made available.

For the monitoring of gaseous and solid by-products, optical-fibre chemical sensing represents an attractive alternative to techniques such as mass and optical spectrometry, gas chromatography, actinometry and ellipsometry. Optical fibre systems are potentially more compact, rugged and better suited for field use. For application to high-voltage switchgear, they also offer the important advantage of not requiring bulky electrical insulation, because of the dielectric nature of optical fibres.

Optical fibre sensors for the detection of gas species can be based on several effects, the most commonly used being fluorescence, optical absorption, surface plasmon resonance, evanescent wave spectroscopy, and absorption of gas by solid films (Dakin and Culshaw 1988). Some of the arrangements use interferometric techniques to enhance the sensor sensitivity.

Recent interest has been generated by the class of evanescent wave sensors that make use of sol-gel derived porous materials. The sol-gel process is a method of fabricating porous glasses by room temperature reaction of organic precursors. Dye molecules or other chemicals can be incorporated into the glass matrix during the process, in order to establish the desired photo-chemical characteristics (MacCraith *et al.* 1991). The nanometre-scale structure of the microporous glass allows interaction between the absorbed species and the immobilised reagents over a large equivalent surface. It also allows chemical selectivity based on molecular size.

In a single-mode silica optical fibre, the evanescent field associated with the guided electromagnetic field is confined to a sub-micrometre region surrounding the fibre core. To achieve interaction between the evanescent field and a sol-gel film, the fibre is first tapered by heating it while applying a tensile stress, until a central diameter of a few micrometres is achieved. In this central region the core diameter is negligible and light is entirely guided by the cladding. The evanescent field extends into the surrounding medium, and can therefore interact with any substance deposited on the fibre. Monitoring of specific chemical species can be achieved by coating the tapered section with a sol-gel film doped with an appropriate analyte-sensitive chemical.

An example of an evanescent wave sensor using a sol-gel glass is the optical fibre oxygen sensor reported by MacCraith *et al.* (1993). In this case, a ruthenium complex is added to the porous glass film surrounding the fibre. The evanescent field associated with the guided light at a wavelength of 488 nm excites the ruthenium complex. The resulting fluorescence is partially coupled back into the fibre and is eventually detected by a photomultiplier. When the sensor is exposed to oxygen, the gas is absorbed by the porous film and quenches the fluorescence, causing a decrease in the output signal.

As part of our own research programme, we have obtained some promising results from preliminary experiments which use a tapered optical fibre to monitor deposition of solid by-products produced during SF_6 glows. The technique uses a single-mode optical fibre passed into and out of the discharge chamber using vacuum feed-throughs. An 80 mm length of the fibre within the chamber has its cladding layer tapered to expose a short length of the fibre core. White light is launched into one end of the fibre and its spectrum monitored at the other end. The effects of absorption on the output spectrum can be analysed to provide information on the nature of the deposited material.

6. Summary and Conclusions

This review of the optical fibre sensing of electrical discharges clearly demonstrates the potential for the technique in the discharge area. The substantial amount of work already completed in the general field of optical fibre sensing, combined with the versatility of the technique, ensures that most discharge parameters are capable of measurement using optical fibres. A major attraction of fibres for discharge work is their immunity to high voltage and electromagnetic radiation. This is particularly significant for measurements on pulsed and r.f. discharges.

Many discharge parameters have not been considered in this review. For example, no surface phenomena have been examined. Processes such as plasma deposition and sputtering could be investigated by chemical fibre sensing, with tapered fibres being used to measure rates of material transfer. Nor have we examined any breakdown processes. These have the potential to be studied using arrays of interferometric sensing fibres which would allow breakdown paths to be tracked, as the streamer and leader discharges produce localised heating of fibres.

Commercial exploitation of the optical fibre sensing of electrical discharges will most likely come about in the power supply industry, where monitoring must be carried out in adverse environments involving high voltages and electromagnetic radiation. Many of the systems and devices employed in the generation and transmission of electricity involve gas discharges, either as part of the controlling mechanism in devices such as circuit breakers and surge arrestors, or in the form of spurious coronas or partial discharges in transformers and on transmission lines. By monitoring parameters associated with these discharges and their effects, data are obtained which provide information on the status of systems and devices, and thus allow informed decisions to be made on maintenance and replacement.

Optical fibre sensors have a number of further characteristics which will encourage their application to power-system monitoring. These include: (i) the convenience of multiplexing, enabling a range of parameters, devices or systems to be monitored simultaneously; (ii) the viability of central monitoring, since optical signal transfer over large fibre lengths can be achieved conveniently, economically and with low loss; and (iii) the versatility of application, which will allow the simultaneous monitoring of critical non-discharge parameters, such as current, voltage and those associated with switchgear hydraulics.

Acknowledgments

This work is supported by grants from the Australian Research Council (ARC) and the Electricity Supply Association of Australia/Energy Research and Development Corporation (ESAA/ERDC) Joint Research Program. The authors are appreciative of the support of their colleagues in the Optical Fibre Sensors group; Graham Hyde, Tim Priest and Dragan Vukovic.

References

Asakawa, Y. (1976). *Nature* **261**, 220.
Bracewell, R. (1965). 'The Fourier Transform and its Applications' (McGraw–Hill: New York).
Bradley, R. F., and Hoburg, J. F. (1985). *IEEE Trans. Ind. Applic.* **IA-21**, 1373.
Chandler, G. I., and Jahoda, F. C. (1985). *Rev. Sci. Instrum.* **56**, 852.
Curry, A. D. (1987). *Chemtech*, Jan., 35.
Dakin, J., and Culshaw, B. (1988). 'Optical Fiber Sensors', Vol. 2, Chap. 16 (Artech House: Boston).
Drain, L. E. (1980). 'The Laser Doppler Technique' (Wiley: New York).
Francis, G. (1956). *In* 'Handbuch Der Physik' (Ed. S. Flugge), Vol. XXII, pp. 53–208 (Springer: Berlin).
Huddlestone, R. H., and Leonard, S. L. (1965). 'Plasma Diagnostic Techniques' (Academic: New York).
Jackson, D. A. (1985). *J. Phys.* E **18**, 981.
Jin, Z. J., Chan, C., and Whitaker, C. (1988). *Rev. Sci. Instrum.* **59**, 427.
Kibler, K. G., and Carter, H. G., Jnr (1974). *J. Appl. Phys.* **45**, 4436.
Kulacki, F. A., and Daumenmier, J. A. (1978). *J. Electrostatics* **5**, 325.
Lamb, D. W., and Woolsey, G. A. (1994). *Appl. Optics*, in press.
Large, M. I., and Pierce, E. T. (1957). *J. Atmos. Terr. Phys.* **10**, 251.
Lassing, H. S., Mastop, W. J., van der Meer, A. F. G., and Oomens, A. A. M. (1987). *Appl. Optics* **26**, 2456.
MacCraith, B. D., McDonagh, M., O' Keeffe, G., Keyes, E. T., Vos, J. G., O'Kelly, B., and McGilp, J. F. (1993). *Analyst* **118**, 385.
MacCraith, B. D., Ruddy, V., Potter, C., O'Kelly, B., and McGilp, J. F. (1991). *Electron. Lett.* **27**, 1247.
Sato, T. (1980). *J. Electrostatics* **8**, 271.
Scelsi, G. B., Everett, V., and Woolsey, G. A. (1994). *In* 'Fibre Optic and Laser Sensors XII' (Ed. R. P. DePaula), Proc. SPIE 2292 (in press).
Sigmund, R. S. (1982). 7th Int. Conf. Gas Discharges and Their Applications, London, p. 140.
Simons, T. D. (1984). *Appl. Optics* **23**, 1807.
Teisseyre, Y., Haug, R., and Ballereau, P. J. (1982). *J. Phys.* D **15**, 1231.
Thanh, L. C. (1979). *Electron. Lett.* **15**, 57.
Wolthuis, R. A., Mitchell, G. L., Saaski, E., Hartl, J. C., and Afromowitz, M. A. (1991). *IEEE Trans. Biomed. Eng.* **38**, 974.
Woolsey, G. A., Lamb, D. W., and Woerner, M. C. H. (1991). *In* 'Fiber Optic and Laser Sensors IX' (Eds R. P. DePaula and E. Udd), Proc. SPIE 1584, p. 243.
Yabe, A., Mori, Y., and Hijikata, K. (1978). *Amer. Inst. Aeronautics Astronautics J.* **16**, 340.

Manuscript received 11 October, accepted 16 November 1994